The Two-Dimensional Hermite S-method for High Resolution ISAR Imaging Applications

Srdjan Stanković, Irena Orović, and Andrey Krylov

Abstract— **The two-dimensional multiwindow S-method for radar imaging applications is proposed. It represents a combined technique that uses the standard S-method and the multiple windows approach based on the two-dimensional Hermite functions. The proposed method provides significant improvement of radar image concentration in comparison with the standard S-method. Also, it does not require an additional post-processing algorithm. The efficiency of the proposed method is demonstrated on various examples.**

I. INTRODUCTION

The Fourier transform is one of the most frequently used signal analysis tool that provides characterization and interpretation of signals for various applications. Hence, in radar imaging, the two-dimensional Fourier transform has been frequently employed. Namely, by applying the two-dimensional Fourier transform to the coherently processed radar echoes, the corresponding radar images are obtained [1]-[4]. It is used for both the synthetic aperture radar (SAR) and the inverse synthetic aperture radar (ISAR) systems. However, the high image resolution can be achieved only in the case of stationary targets in SAR and constant rotation in ISAR applications. Otherwise, the Doppler shift and the Doppler spread in the received signal will cause blurred and smeared images. Therefore, in order to improve the resolution in these cases, various time-frequency approaches [5]-[8] and/or motion compensation techniques have been employed [9], [10]. The motion compensation techniques provide good results usually by estimating target motion parameters, but at the expense of high computational load. Concerning the time-frequency representations, some efficient solutions have been provided by using the S-method [5], [6], [8]. It provides highly concentrated representation as in the case of the Wigner distribution, but with reduced number of cross-terms [11]. The S-method is computationally very efficient technique that starts from the two-dimensional Fourier transform and improves its concentration by performing a simple convolution within the frequency domain window. The appropriate selection of window width is crucial for image resolution and readability. The narrow window may produce the blurred radar image, while in the case of wide window, the cross-terms appear. More details about the choice of window width can be found in [7], [11]. To provide satisfactory results, in some cases the S-method is combined with an additional post-processing algorithm [8].

In order to improve performances of the Fourier transform and the standard S-method in radar imaging, the two-dimensional multiwindow S-method is introduced in this paper. It can be considered as an extension of the method introduced in [8]. The proposed multiwindow approach is based on the usage of two-dimensional Hermite functions. These functions exhibit some desirable properties such as good time-frequency localization: they are optimally concentrated in the circular region$R = \{(t, f) : t^2 + f^2 \leq C\}$, with C a constant. A signal expansion into series of Hermite functions provides, at the same time, the insight to its Fourier transform, since they are the eigenfunctions of the Fourier transform. Therefore, the two-dimensional Hermite functions are combined with the advantages of the S-method, providing an enhanced resolution in radar imaging. Our approach uses

IET Signal Processing, Vol. 4, No. 4, Jan. 2010.

only a few low order functions, and hence the algorithm complexity is slightly increased in comparison with the standard S-method. Unlike some common time-frequency techniques, that split the ISAR image into a time-series of ISAR images, the multiwindow S-method uses the whole set of data, in the same way as the standard S-method does [7], [12]. It starts with an already obtained radar image, based on the multiwindow Fourier transform, and improves its concentration by additional matrix calculations.

The paper is organized as follows. Brief review of the basic radar signal model and ISAR model is given in Section II. In Section III, the multiwindow Hermite S-method is proposed. The experimental results including the ISAR application are presented in Section IV. Concluding remarks are given in Section V.

II. Theoretical Background – Signal Model and ISAR Model

The commonly used techniques for radar imaging are SAR and ISAR. These methods are designed to provide high resolution images of stationary and moving targets. The SAR method is used for stationary targets while the radar is moving at a uniform speed and at a constant altitude [3]. On the other hand, the ISAR method is designed for moving target while the radar is fixed. In both systems, radar transmits a signal usually in the form of M coherent chirps [3], [6]:

$$x_{T_x}(t) = e^{-j\omega_0 t} \sum_{m=0}^{M-1} x_a(t - mT_r), \quad (1)$$

where:

$$x_a(t) = \begin{cases} e^{j\pi B f_r t^2} & for \quad 0 \le t \le T_r \\ 0 & otherwise. \end{cases} \quad (2)$$

The model parameters are:
1. t: Fast time,
2. ω_0: Radar operating frequency,
3. T_r: Pulse repetition rate
4. mT_r: Indexes the slow time
5. MT_r: Total signal duration
6. $f_r = 1/T_r$: Repetition frequency
7. B: Bandwidth of the transmitted pulse.

Assuming that the distance between the radar and the target is d (also known as the range), the received signal is delayed with respect to the transmitted signal by $2d/c$, as follows:

$$x_{R_x}(t) = \sigma e^{-j\omega_0(t-2d/c)} \sum_{m=0}^{M-1} x_a(t - \frac{2d}{c} - mT_r), \quad (3)$$

where σ is the reflection coefficient, while c is the speed of light. The received baseband signal produced by the m-th chirp and returned from the single point scatterer can be written as [6], [7]:

$$x_{R_x}(m,t) = \sigma e^{j\omega_0 2d/c} e^{-j2\pi B f_r (t - mT_r) 2d/c}. \quad (4)$$

Using the matched filtering of the m-th received pulse and the m-th transmitted pulse (the received signal is multiplied with the complex conjugate of the transmitted signal), produces:

$$x(m,t) = \sigma e^{j\omega_0 2d/c} e^{j2\pi B f_r (t - mT_r)} e^{j\pi B f_r \left(\frac{2d}{c}\right)^2}. \quad (5)$$

Since $B \ll \omega_0$, the constant phase shift $e^{j\pi B f_r 4\frac{d^2}{c^2}}$ can be neglected with respect to other two components [9]. Thus, by substituting $t - mT_r = nT_s$ into (5), where T_s is the sampling interval within the chirp, the two-dimensional discrete mixed signal can be obtained in the form [6], [7]:

$$x(m,n) = \sigma e^{j\omega_0 2d/c} e^{-j\theta n}, \quad (6)$$

where $\theta = 2\pi B f_r 2d/cT_s$ is the angular frequency. The Fourier transform will result in a pulse at the angular frequency θ, proportional to the range d. Note that, in the case of target that is moving with respect to radar, the range is time dependent: $d(t) = d(nT_s + mT_r)$.

ISAR model: Let us assume that a location of the p-th target point scatterer is (x_p, y_p). The range coordinate (in direction of the radar-target line) is denoted by x_p, while y_p denotes the cross-range coordinate (in the direction normal to the radar-target line). The total range of the p-th scatterer is then defined as [7]:

$$d(t) = R(t), \quad R = R_0,$$

$$R(t) = R_0 + x_p \cos(\omega_R t) + y_p \sin(\omega_R t)$$
$$\lim_{\omega_R \to 0}[R(t)] = R_0 + x_p + y_p \omega_R t, \quad (7)$$

where $\omega_R t$ is the rotation angle of point scatterer. The Doppler shift is obtained as [7]:

$$\omega_d = \frac{2\omega_0}{c}\frac{d}{dt}[d(t)] =$$

$$= \frac{2\omega_0}{c}\frac{d}{dt}[R_0 + x_p \cos(\omega_R t) + y_p \sin(\omega_R t)], \quad (8)$$

For $\omega_R t \to 0$, $\omega_d = \frac{2\omega_0}{c} y_p \omega_R \sim y_p$ holds, assuming that the translation is compensated. According to these conditions, $d(t) \approx x_p$, while the velocity is $v(t) \approx y_p \omega_R = v$.
Under previous assumptions, the two- dimensional Fourier transform of the signal corresponding to the p-th scatterer can be approximated by [9]: $2\pi\sigma_p \delta(\omega_t - c_1 y_p)\delta(\omega_m - c_2 m x_p)$, where $c_1 = 2\omega_R\omega_0/c$and $c_2 = 4\pi B/c$. In other words, it produces a peak on the proper scatterer position.

Non-uniform motion: When the target rotates with constant angular velocity ω_R, for a longer period of time, the position of p-th scatterer is given by: $y_p = r_p \sin(\omega_R t)$, $x_p = r_p \cos(\omega_R t)$,where $r_p = \sqrt{x_p + y_p}$. Hence, for the time interval $[t, t+\Delta t]$, the cross-range coordinate changes within the interval [7]:

$$[y_p, y_p + \Delta y_p] =$$

$$= [r_p \sin(\omega_R t), x_p \sin(\omega_R \Delta t) + y_p \cos(\omega_R \Delta t)]. \quad (9)$$

The line-of-sight projection of the point scatterer velocity changes within:

$$[v_s(t), v_s(t+\Delta t)] =$$

$$= [r_p \omega_R \sin(\omega_R t), r_p \omega_R \sin(\omega_R (t+\Delta t)] =$$

$$= [y_p \omega_R, x_p \omega_R \sin(\omega_R \Delta t) + y_p \omega_R \cos(\omega_R \Delta t)]. \quad (10)$$

Furthermore, for small $\omega_R \Delta t$, (10) can be written as [7]:

$$[v_s(t), v_s(t+\Delta t)] = [y_p \omega_R, y_p \omega_R + x_p \omega_R \Delta t]. \quad (11)$$

Thus, at the frequency that corresponds to$y_p \omega_R$, a function corresponding to the linear frequency modulated signal is obtained instead of delta pulse [7]. The same holds for the range coordinate x_p. If $\omega_R \Delta t$is not small enough, or if $\omega_R$is not constant, the instantaneous frequency can be highly non-linear, resulting in a spread two-dimensional Fourier transform and blurred image.

III. Time-Frequency Analysis in ISAR: Two-Dimensional Multiwindow S-method

A. The Two-dimensional Fourier Transform and the S-method

The two-dimensional Fourier transform has been widely used in radar imaging. For the received signal $x(m,n)$, it is given in the form:

$$X(p,q) = \sum_{m=0}^{M-1}\sum_{n=0}^{N-1} x(m,n) e^{-j(2\pi mp/M + 2\pi nq/N)}. \quad (12)$$

The ISAR image is obtained by using the periodogram, defined as $Per(p,q) = |X(p,q)|^2$, which is the square modulus of the Fourier transform. Due to the nonuniform target motions, the Doppler shift corresponding to the cross-range of each scatterer, is time-varying. The received radar signal will be frequency modulated. Consequently, its two-dimensional Fourier transform will be spread, resulting in the blurred or smeared image.

In order to improve the concentration of the periodogram, the S-method has been used. The S-method for a fixed range cell is defined as [6], [11]:

$$SM_R(p,q) = \sum_{i=-L}^{L} P(i) X(p+i,q) X^*(p-i,q), \quad (13)$$

where $P(i)$ is a frequency window which is commonly of rectangular form. Similarly, for a fixed cross-range cell, the S-method can be written as:

$$SM_{CR}(p,q) = \sum_{j=-L}^{L} P(j) X(p,q+j) X^*(p,q-j). \quad (14)$$

Consequently, the two-dimensional S-method that improves the concentration of radar images along both coordinates (range and cross-range) is defined as [6], [13]:

$$SM(p,q) =$$

$$= \sum_{i=-L}^{L}\sum_{j=-L}^{L} P(i,j)X(p+i,q+j)X^*(p-i,q-j)$$

$$= Per(p,q)+$$

$$+2Re\left\{\sum_{i=1}^{L}\sum_{j=1}^{L} P(i,j)X(p+i,q+j)\times\right.$$

$$\left.\times X^*(p-i,q-j)\right\}. \quad (15)$$

Note that, in some applications, the one-dimensional S-method applied to the cross-range coordinate could provide satisfactory results [8]. Namely, the target velocities induce spreading in the cross-range and focusing along this axis is needed. However, as a result of nonuniform rotation (or fast movements) performed by the target and radar setup, the spreading may appear along the range axis as well. In this case the two-dimensional S-method can be used [8].

The S-method is very suitable for hardware realization and some efficient solutions have already been proposed and analyzed in [14], [15].

B. The multiwindow S-method based on the Hermite functions

Spatial function in the Sturm-Liouville boundary value problem, which appears, for example, in the treatment of the harmonic oscillator in quantum mechanics, is called Hermite function [16]. The Hermite functions are the eigenfunctions of the Fourier transform:

$$FT(\Psi_k(x)) = i^k\Psi_k(x), \quad (16)$$

where $FT(.)$ denotes the Fourier transform. Thus, an expansion of signal into a series of Hermite functions enables one to analyze of the signal and its Fourier transform simultaneously. Furthermore, the Hermite functions are orthogonal and well localized in both time and frequency domains. Hence, the set of Hermite functions could be employed for efficient time-frequency analysis. The two-dimensional Hermite functions are defined as follows [16], [17]:

$$\Psi_{kl}(x,y) =$$

$$= \frac{(-1)^{k+l}e^{x^2/2+y^2/2}}{\sqrt{2^{k+l}k!l!\pi}}\frac{d^k(e^{-x^2})}{dx^k}\frac{d^l(e^{-y^2})}{dy^l}. \quad (17)$$

Some examples of two-dimensional Hermite functions are plotted in Fig 1. It is interesting to note that a two-dimensional Hermite function can be obtained by calculating one-dimensional Hermite functions for each coordinate separately:

$$\Psi_{kl}(x,y) = \Psi_k(x)\Psi_l(y) =$$

$$= \frac{(-1)^k e^{x^2/2}}{\sqrt{2^k k!\sqrt{\pi}}}\frac{d^k(e^{-x^2})}{dx^k}\frac{(-1)^l e^{y^2/2}}{\sqrt{2^l l!\sqrt{\pi}}}\frac{d^l(e^{-y^2})}{dy^l}. \quad (18)$$

Although they seem to be complex for realization, the Hermite functions could be easily calculated by using the recursive realization as follows [18]:

$$\Psi_0(x) = \frac{1}{\sqrt[4]{\pi}}e^{-x^2/2},$$

$$\Psi_1(x) = \frac{\sqrt{2}x}{\sqrt[4]{\pi}}e^{-x^2/2},$$

$$\Psi_k(x) = x\sqrt{\frac{2}{k}}\Psi_{k-1}(x)-$$

$$-\sqrt{\frac{k-1}{k}}\Psi_{k-2}(x), \ \ \forall k \geq 2. \quad (19)$$

In order to improve the concentration in the time-frequency domain, the Hermite functions have been used in the definition of multiwindow spectrograms, denoted as $HSpec(t,\omega)$ [19]-[21], which could be written in the discrete form as:

$$HSpec(n,\omega) =$$

$$= \sum_{k=0}^{K-1}\left(\sqrt{d_k}\left|\sum_m x(m)\Psi_k(m-n)e^{-j\omega m}\right|\right)^2, \quad (20)$$

where d_k are the weighting coefficients. It has been shown that the multiwindow spectrogram outperforms the standard one and can provide highly concentrated time-frequency representation [20], [21]. Similarly, to improve the concentration of radar images, the multiple windows approach based on the Hermite functions can be adapted for two-dimensional case and the existing processing tools: the two-dimensional Fourier transform and the S-method (the one-dimensional and two-dimensional cases).

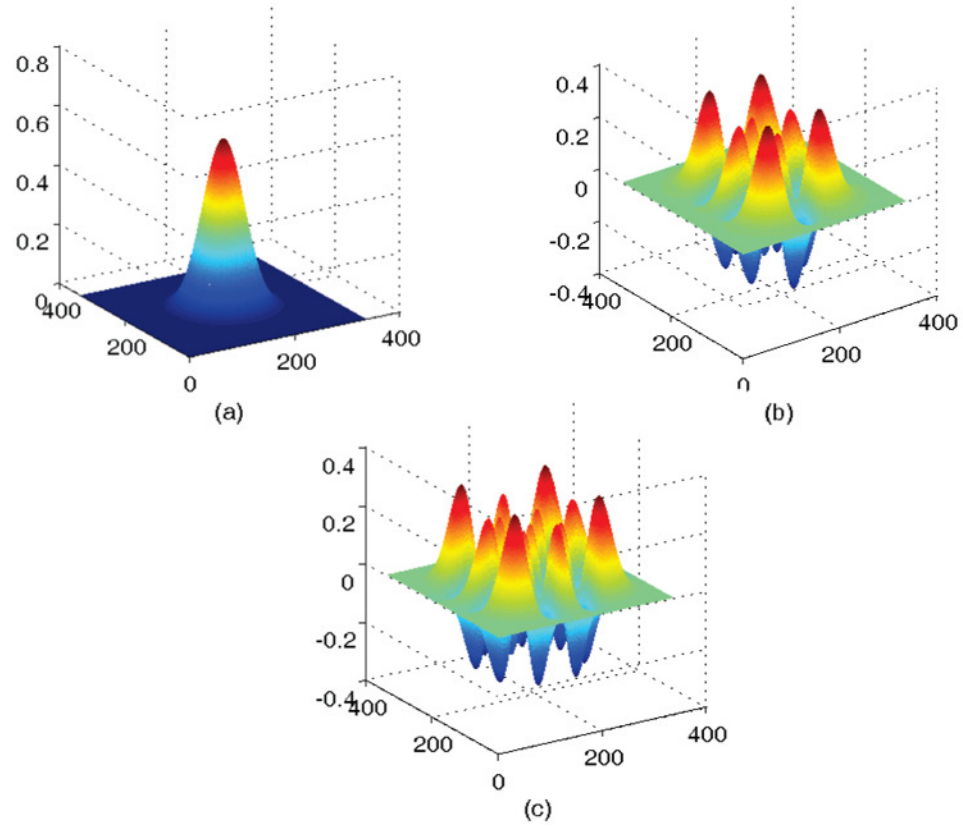

Fig. 1. Illustrations of some two-dimensional Hermite functions: a) $\Psi_{00}(x,y)$, b)$\Psi_{24}(x,y)$, c)$\Psi_{44}(x,y)$

Analogous to the standard S-method, the two-dimensional multiwindow S-method can be defined as a convolution of Hermite based Fourier transforms, as follows:

$$HSM(p,q) =$$

$$= \sum_{i=-L}^{L} \sum_{j=-L}^{L} P(i,j) HX^{K}(p+i,q+j) \times$$

$$\times HX^{K*}(p-i,q-j), \qquad (21)$$

where $HX^{K}(p,q)$denotes the multiwindow two-dimensional Fourier transform. It is obtained as a sum of two-dimensional Fourier transforms calculated by using two-dimensional Hermite functions of various orders, as follows:

$$HX^{K}(p,q) = \sum_{k=0}^{K-1} \sum_{l=0}^{K-1} HX^{kl}(p,q) =$$

$$= \sum_{k=0}^{K-1} \sum_{l=0}^{K-1} \sum_{m=0}^{M-1} \sum_{n=0}^{N-1} d_{k_l} \Psi_{kl}(m,n)$$

$$\times x(m,n) e^{-j(2\pi mp/M + 2\pi nq/N)}. \qquad (22)$$

where d_{kl} are the weighting coefficients, while K is the number of functions used along both range and cross-range direction (axis). Furthermore, in order to simplify the realization, $HX^{kl}(p,q)$ is obtained as a composition of one-dimensional cases, as follows:

$$HX^{kl}(p,q) = \sum_{n=0}^{N-1} \left[\sqrt{d_l} \Psi_l(n) e^{-j2\pi np/N} \right.$$

$$\left. \times \sum_{m=0}^{M-1} \sqrt{d_k} \Psi_k(m)\, x(m,n) e^{-j2\pi mq/M} \right]. \qquad (23)$$

The one-dimensional weighting coefficients d_k and d_l are determined according to the procedure described in [21], while $d_{kl}=\sqrt{d_k d_l}$ =

d_{lk} holds. The different order Hermite functions act as multiple windows that improve the concentration in both directions.

The two-dimensional multiwindow periodogram is obtained as: $HPer(p,q) = \sum_{k=0}^{K-1} \sum_{l=0}^{K-1} \left|HX^{kl}(p,q)\right|^2$.
Consequently, the multiwindow Hermite S-method can be written in the form:

$$HSM(p,q) = HPer(p,q) + \\ +2Re\left\{\sum_{i=1}^{L}\sum_{j=1}^{L} P(i,j) HX^{K}(p+i,q+j) \right. \\ \left. \times HX^{K*}(p-i,q-j)\right\} \quad (24)$$

Observe that in case of the standard S-method given by (15), the terms $2Re$ $\left\{\sum_{i=1}^{L}\sum_{j=1}^{L} P(i,j)X(p+i,q+j)\right.$ $\left.\times X^*(p-i,q-j)\right\}$ are used to improve the periodogram concentration (all even phase derivatives are removed from the spread factor) [6], [8]. Since the same idea is used for multiwindow approach, the multiwindow S-method improves the resolution by eliminating even phase derivatives that remain after the multiwindow periodogram removed first K-1 derivatives [21].

In some applications, it might be sufficient to calculate the Hermite S-method along only one axis. Thus, the Hermite S-method in range and cross-range direction could be, respectively, defined as:

$$HSM_R(p,q) = \\ = \sum_{i=-L}^{L}\sum_{j=-L}^{L} P(i,j) HX^{K}(p+i,q) HX^{K*}(p-i,q),$$

$$HSM_{CR}(p,q) = \\ = \sum_{i=-L}^{L}\sum_{j=-L}^{L} P(i,j) HX^{K}(p,q+j) HX^{K*}(p,q-j). \quad (25)$$

The proposed approach can be generalized by using other functions instead of the Hermite functions. For example, the Laguerre functions could be interpreted as the Wigner distribution of Hermite functions (k-th order Laguerre function is the Wigner distribution of the k-th order Hermite function), and hence, could be used to generate optimal kernels [20]. Furthermore, the windows provided by spline functions, e.g. B-spline functions that are time-limited piecewise polynomials [22], could be considered, as well.

IV. Example

Example 1: In order to demonstrate how the S-method improves the concentration in the time-frequency domain, let us observe the simple simulated signal in the form:

$$x(n) = x_1(n) + x_2(n) + x_3(n) + x_4(n),$$

where,

$$x_1(n) = A(n)e^{j\frac{0.2}{256}\pi n^2}e^{j\frac{\pi}{2}n},$$

$$x_2(n) = A(n)e^{j\frac{0.24}{256}\pi n^2}e^{j\frac{\pi}{8}n},$$

$$x_3(n) = A(n)e^{-j\frac{0.18}{256}\pi n^2}e^{-j\frac{\pi}{4}n},$$

$$x_4(n) = A(n)e^{-j\frac{0.12}{256}\pi n^2}e^{-j\frac{\pi}{2}n}.$$

The time instant n=0 is considered. Thus, the signal consists of four components that may correspond to the returned radar signals from four point targets that accelerate. The amplitude is slow-varying: $A(n) = \frac{1}{2} + \frac{1}{2}\cos\frac{\pi}{256}n$, $-128 \le n \le 127$.The discrete instantaneous frequencies of signal components are: $\omega_1(0) = \frac{\pi}{2}$,$\omega_2(0) = \frac{\pi}{8}$,$\omega_3(0) = -\frac{\pi}{4}$ and $\omega_4(0) = -\frac{\pi}{2}$. The Hermite S-method is calculated by using different values of parameter L (L=0, 4, 16, 32), and the results are shown in Fig 2. Here, the same number of Hermite functions: K=3 is used for each L. One might observe that the concentration of signal components increases by increasing L, i.e. by increasing the number of convolution terms in the Hermite S-method. However, for high values of L (L=16 and L=32 in Fig 2), the undesired cross-terms appear between components. Generally, in most applications, $3 \le L \le 10$ should be used [7], [11].

Furthermore, the concentration can be also improved by increasing the number of Hermite functions K. The Hermite S-method, implemented by using different number of Hermite functions (K=1, 2, 3, and 4) is illustrated in

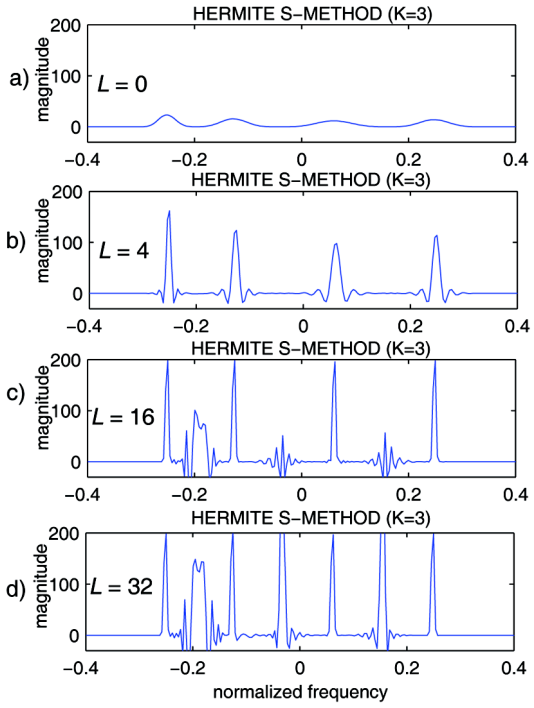

Fig. 2. Concentration improvement by increasing L: a) L=0, b) L=4, c) L=16, d) L=32

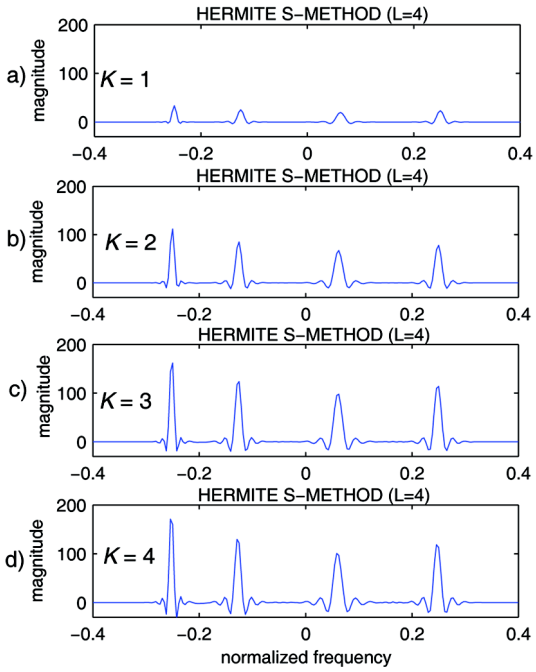

Fig. 3. Concentration improvement by increasing K: a) K=1, b) K=2, c) K=3, d) K=4

Fig 3. Note that the same value of parameter L (L=4) is used for all values of K.

Example 2: In order to prove efficiency of the Hermite S-method in target points detection, the simulated range/cross-range data are used. The radar setup assumes: high resolution radar operating at the frequency f_0=10.1GHz, bandwidth of the transmitted signal B=600MHz, the coherent integration time T=2s, 64 pulses in one revisit and 256 samples within one pulse. The target is at 2 km distance from the radar and rotates at $\omega_R = 2.1^0/\text{sec}$. The nonlinear rotation with frequency $\Omega = 0.5Hz$ is superimposed:$\omega_R(t) = \omega_R + A\sin(2\pi\Omega t)$, where $A = 1.05^0/\text{sec}$. The translation is not assumed within the experiment, so there is no need for translation compensation. The target is simulated as six point scatterers in (x, y) plane, where the positions of scatterers at t=0 are: (x_1, y$_1$)=(-2.1, 1.44), (x_2,y$_2$)=(0, 1.44), (x_3,y$_3$)=(2.1, 1.44), (x_4,y$_4$)=(-1.08, -0.72), (x_5,y$_5$)=(1.08, -0.72), (x_6,y$_6$)=(0, -2.28). All coordinates are in meters. Radar images obtained by using: the two-dimensional Fourier transform (periodogram), the standard S-method and the proposed Hermite S-method are given in Fig 4. The parameter L=3 is used for the calculation of both the S-method and the Hermite S-method. The number of Hermite functions used in the Hermite S-method is K=3.

We have calculated the number of "correct points" by finding the six largest values within the periodogram, the S-method and the Hermite S-method (Fig 5), and checking if they correspond to the true targets positions. Other points are set to zero. The coordinates of the six points with largest energy are given in Table I. Note that in the case of periodogram, the selected points are quite dislocated from the true target points. Four out of six points could be considered as "correct points", if the S-method is used, while all selected points in the Hermite S-method are "correct points" for this signal.

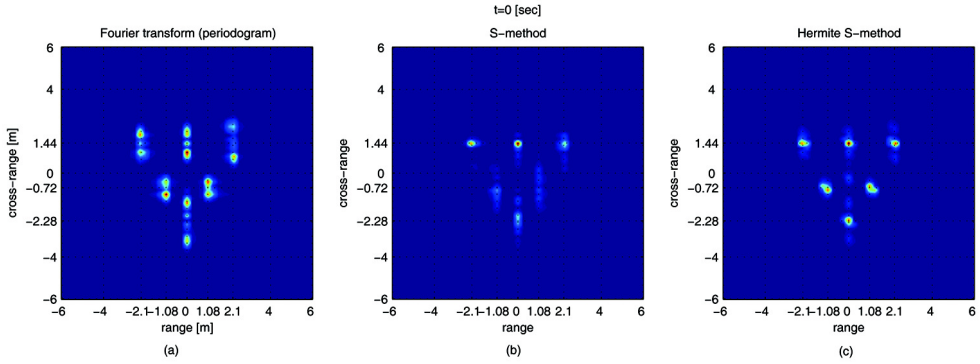

Fig. 4. ISAR images of simulated range/cross-range data: a) periodogram, b) standard S-method, c) Hermite S-method

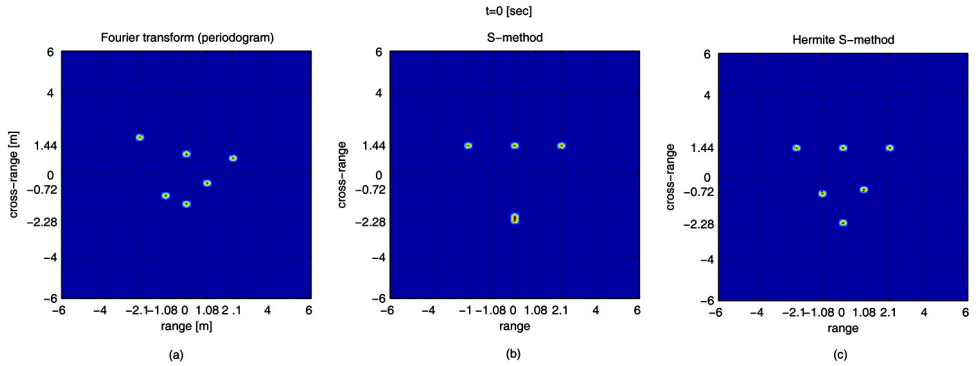

Fig. 5. Six largest values (points) within: a) periodogram, b) standard S-method, c) Hermite S-method

TABLE I
THE COORDINATES OF SIX LARGEST POINTS

(x,y)	i=1	i=2	i=3	i=4	i=5	i=6
True points	(-2.1, 1.44)	(0, 1.44)	(2.1, 1.44)	(-1.08, -0.72)	(1.08, -0.72)	(0, -2.28)
Periodogram	(-2.25, 1.82)	(0, 1)	(2.25, 0.8)	(-1, -1)	(1, -0.4)	(0, 1.4)
S-method	(-2.2, 1.44)	(0, 1.44)	(2.2, 1.44)	(0, 2)	(0,2.1)	(0, 2.2)
Hermite S-method	(-2.2, 1.44)	(0, 1.44)	(2.2, 1.44)	(-1,-0.8)	(1, -0.65)	(0, -2.28)

Furthermore, all points whose energy is above the minimal energy of true points are considered as "false alarms". In Fig 6, we have illustrated the true points and "false alarms". The number of "false alarms" in the case of periodogram and S-method is 8 (in total 14 point are presented). Note that within the Hermite S-method there are no "false alarms" in this example.

Example 3: The MIG target model is used in this example. The ISAR images of MIG25, obtained by using standard periodogram and the standard S-method (without post-processing algorithms and by using the rectangular window), are shown in Fig 7.a and b, respectively. The value of parameter L=3 is used in the calculation of the standard S-method. Note that some parts of the ISAR images are blurred due to the maneuvers that target performs (for example the points on the nose, wings, etc). The standard S-method cannot provide notable improvement of the concentration, since the starting two-dimensional Fourier transform produces quite

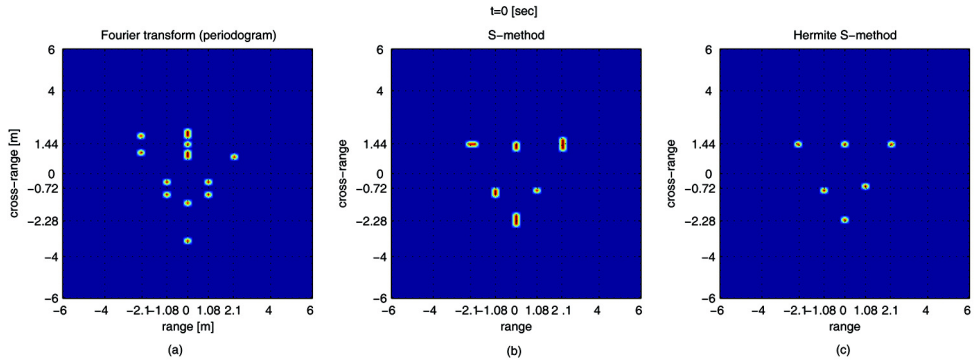

Fig. 6. True target points and "false alarms": a) periodogram, b) standard S-method, c) Hermite S-method

unfocused image.

In Fig 7.c the two-dimensional Hermite periodogram is shown. It is obtained by using the two-dimensional Hermite functions for K=3 (three Hermite functions are used in both range and cross-range direction). Its concentration can be further improved by using the Hermite S-method. Hence, the images obtained by using the Hermite S-method for K=1 (one window function in both range and cross-range directions) and K=3 (three window functions are used in both range and cross-range directions) are shown in Figs 7.d and 7.e, respectively. As in the case of standard S-method, the parameter L=3 is used for the Hermite S-method calculation. Observe that the image in Fig 7.e (the Hermite S-method for K=3 and L=3) is quite focused and improved comparing to other presented cases (including the case for K=1).

In this example, the one-dimensional form of Hermite S-method applied to cross-range direction is sufficient to provide good results and low computational costs. Namely, the images are sharp enough in the range direction, so the convolution within the standard S-method and the Hermite S-method can be applied only to the cross-range direction. Since a small number of Hermite functions (K=3) is used, this approach is still efficient regarding the computational complexity.

The measure of image sharpness [23] is used in order to quantify the quality of re-focused images. This simple quality metric is defined as the intensity normalized sum of the absolute value of pixel photocurrent convolved with a spatial high pass filter [23]:

$$IQM = \frac{1}{E}\sum_i\sum_j |I_{i,j} * K|\,,$$
$$K = \begin{bmatrix} 0 & -1 & 0 \\ -1 & 4 & -1 \\ 0 & -1 & 0 \end{bmatrix},$$

where $I_{i,j}$ is the intensity at the $(i,j)^{th}$ position and $E = \sum_i\sum_j I_{i,j}$is the total intensity of the image. As an additional objective measure, the image contrast is calculated as follows [24]:

$$C = \frac{\sqrt{\sum_i\sum_j |I_{i,j}|^4}}{\sum_i\sum_j |I_{i,j}|^2}.$$

The quality measures, IQM and C, for images presented in Fig 7, are given in Table II. Note that in the case of image obtained by using the Hermite S-method, the measures IQM and C have the highest values, indicating the highest quality.

Example 4: Here, the simulation with the noisy signal is considered. Namely, the signal from the previous example has been corrupted by the Gaussian noise with SNR=3dB. The ISAR images obtained by using the standard periodogram, the standard S-method, the Hermite periodogram and the Hermite S-method are presented in Fig 8.

Note that the images obtained by using the standard periodogram and the standard S-method are quite blurred and smeared (Fig 8.a

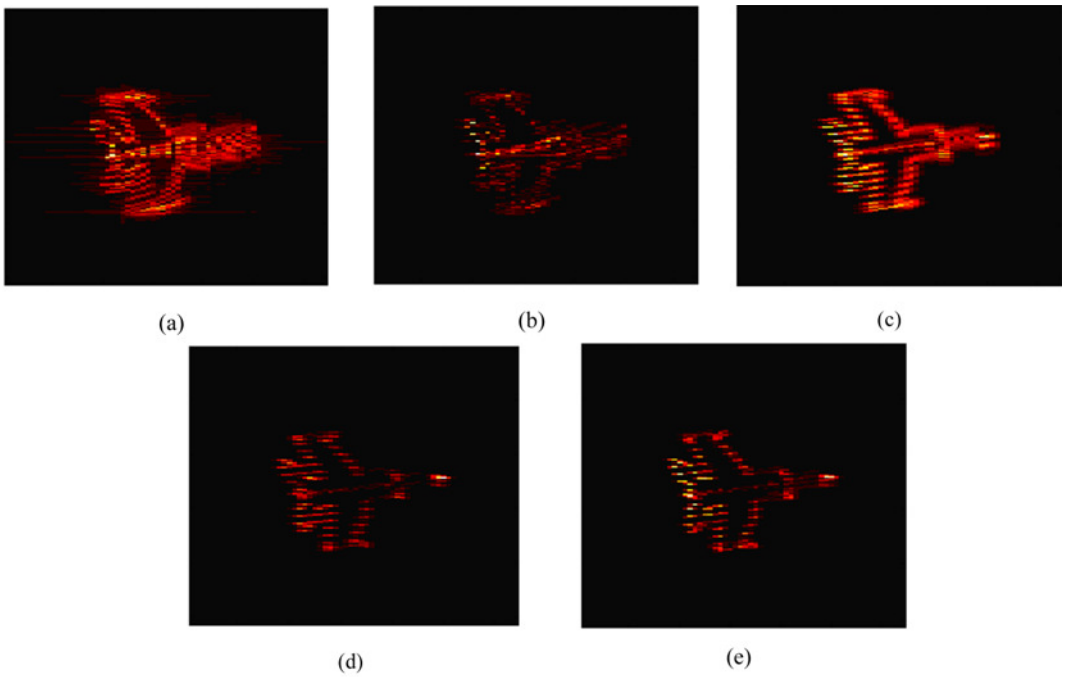

Fig. 7. ISAR image of MIG25 obtained by using: a) two-dimensional Fourier transform, b) standard S-method, c) two-dimensional Hermite periodogram, d) Hermite S-method by using K=1, e) Hermite S-method by using K=3

TABLE II
IMAGE QUALITY METRICS

Image obtained by using:	***IQM***	***C***
Standard periodogram – Fig 7.a	0.76	0.00089
Standard S-method (L=3) - Fig 7.b	0.71	0.0011
Hermite periodogram (K=3) - Fig 7.c	0.79	0.014
Hermite S-method (K=3,L=3) - Fig 7.e	0.86	0.0019

and Fig 8.b, respectively). The Hermite periodogram (Fig 8.c) improves the results, but it is still blurred and affected by the noise. However, the Hermite S-method (Fig 8.d) is more robust in noisy conditions and provides rather clear and focused image.

V. CONCLUSION

A multiwindow Hermite S-method is introduced as an efficient tool for high resolution radar imaging. This multiwindow approach is based on the usage of two-dimensional Hermite functions. Also, the Hermite based two-dimensional Fourier transform and Hermite periodogram are defined as intermediate processing steps. Furthermore, the one-dimensional and two-dimensional versions of the Hermite S-method are considered. The Hermite S-method provides a significant resolution improvement comparing to two-dimensional Fourier transform and the standard S-method. The enhanced resolution could be obtained with only a few Hermite functions that could be easily calculated by using the recursive algorithm. The computational complexity of the proposed method is slightly increased comparing to the standard S-method. Hence, it is amenable for implementation in hardware.

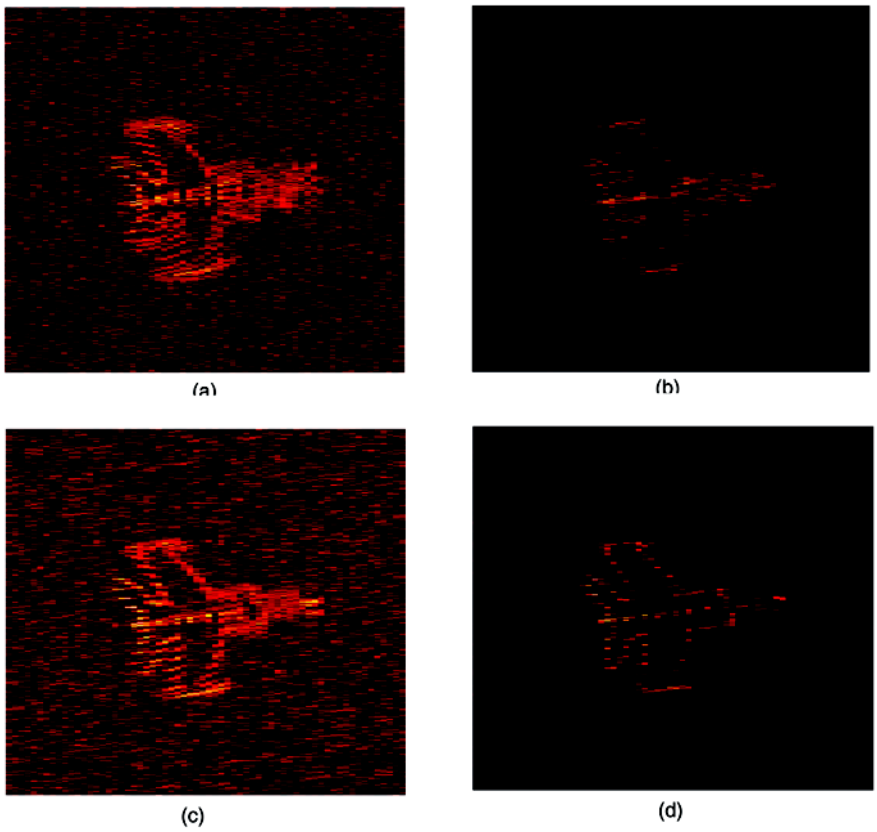

Fig. 8. Noisy ISAR image of MIG25 obtained by using: a) periodogram, b) standard S-method, c) Hermite periodogram, d) Hermite S-method by using K=3

Acknowledgment

The authors are very thankful to anonymous reviewers for useful comments and suggestions that helped to improve the paper.

References

[1] Carrara, W. G., Goodman, R. S., and Majewski, R. M.: 'Spotlight Synthetic Aperture Radar—Signal Processing Algorithms', Artech House, Norwood, Ohio, USA, 1995.

[2] Wong, S., Riseborough, E., and Duff, G.: 'Experimental investigation on the distortion of ISAR images using different radar waveforms', Technical Memorandum TM 2003-196, Defence Research and Development Canada, Ottawa, Canada, 2003.

[3] Chen, V. C., and Ling, H.: 'Time-Frequency Transforms for Radar Imaging and Signal Analysis', Artech House, Boston, Mass, USA, 2002.

[4] DeGraaf, S. R.: 'SAR imaging via modern 2-D spectral estimation methods', *IEEE Transactions on Image Processing*, 1998, 7, 5, pp. 729–761.

[5] Popovic, V., Dakovic, M., Thayaparan, T., and Stankovic, LJ.: 'SAR Image Improvements by Using the S-method', *in Proc.* IEEE *ICASSP*, vol. 3, May 2006, pp.III 177-III 180.

[6] Stankovic, LJ., Thayaparan, T., Dakovic, M., and Popovic, V.: 'S-method in radar imaging', in *Proceedings of the 14th European Signal Processing Conference (EUSIPCO '06)*, Florence, Italy, September 2006.

[7] Thayaparan, T., Stanković , LJ., Wernik, C., and Daković , M.: 'Real-time motion compensation, image formation and image enhancement of moving targets in ISAR and SAR using S-method based approach', *IET Signal Processing*, 2008, 2, 3, pp. 247-264.

[8] Stanković , LJ., Thayaparan, T., Popović , V., Djurović , I., and Daković , M.: 'Adaptive S-method for SAR/ISAR Imaging', *Eurasip Journal on Advanced Signal Processing*, 2008, Article ID 593216, 10 pages.

[9] Djurović , I., Thayaparan, T., and Stanković , LJ.: 'Adaptive Local Polynomial Fourier transform in ISAR', *Eurasip Journal on Applied Signal Processing*, 2006, Article ID 36093, 15 pages.

[10] Haiqing, W., Grenier, D., Delisle, G. Y., and Da-

Gang, F.: 'Translational motion compensation in ISAR image processing', IEEE *Transaction on image processing*, 1995, 4, 11, pp.1561-1571.

[11] Stanković , LJ.: 'A method for Time-Frequency Signal Analysis', IEEE *Transaction on Signal Processing,* 1994, 42, 1, pp. 225-229.

[12] Thayaparan, T., Stanković , L., Daković , M.: "S-method based approach for image formation, motion compensation, and image enhancement of moving targets in ISAR and SAR", *IEEE International Symposium on Geoscience and Remote Sensing*, IGARSS 2008.,vol.2, pp. II-29-II-32, July 2008.

[13] Stanković , S., Stanković , LJ., and Uskoković , Z.: 'On the Local Frequency, Group Shift and Cross Terms in Some Multidinesional Time-Frequency Distributions; A method for Multidimensional Time-Frequency Analysis', *IEEE Transaction on Signal Processing*, 1995, 43, 7, pp. 1719-1724.

[14] Stanković , S., Stanković , LJ., Ivanović , V., and Stojanović , R.: 'An Architecture for the VLSI Design of Systems for Time-Frequency Analysis and Time-Varying Filtering', *Annales des Telecommunications*, 2002, 57, (9/10), pp. 974-995.

[15] Stanković , S., Djurović , I., and Vuković , V.: 'System Architecture for Space-Frequency Image Analysis', *Electronic Letters*, 1998, 34, 23, pp. 2224-2225.

[16] Najafi, M., Krylov, A., and Kortchagine, D.: 'Image Deblocking With 2-D Hermite Transform', *Proceeding Int. Conference Graphicon 2003*, Moscow 2003, pp. 180-183.

[17] Krylov, A., and Kortchagine, D.: 'Hermite Foveation', *Proceeding Int. Conference Graphicon 2004*, pp. 166-169, Moscow, 2004.

[18] Kortchagine, D. N. and Krylov, A. S.: 'Projecton Filtering in image processing', *Proceeding Int. Conference Graphicon 2000*, pp.42-45, 2000.

[19] G. Fraser, B. Boashash, "Multiple window spectrogram and time-frequency distributions," in *Proc. IEEE ICASSP*, vol. 4, 1994, pp. 293-296.

[20] Bayram, M., and Baraniuk, R. G.: 'Multiple Window Time-Frequency Analysis', *Proc. of the IEEE Signal Processing International Symposium on Time-Frequency and Time-Scale Analysis*, pp.173-176, Jun 1996.

[21] Cakrak, F., and Loughin, P. J.: 'Multiwindow Time-Varying Spectrum with Instantaneous Bandwidth and Frequency Constraints', IEEE *Transactions on Signal Processing*, 2001, 49, 8, pp. 1656-1666.

[22] Toraichi, K., Kamada, M., Itahashi, S. and Mori, R.: 'Window functions represented by B-spline functions', IEEE *Trans. on Acoustics, Speech and Signal Processing*, 1989, 37, 1, pp. 145-147.

[23] Cohen, M., Cauwenberghs, G., and Vorontsov, M.: 'Image Sharpness and Beam Focus VLSI Sensors for Adaptive Optics', IEEE *Sensors Journal*, 2002, 2, 6, pp. 680-690.

[24] Callow, H.J., Saebo, T.O., and Hansen, R. E.: 'Towards Robust Quality Assessment of SAS Imagery using the DPCA algorithm', *Oceans 2005 – Europe*, 2005, 2, pp. 1095-1100.